Biomaterials Science

Accepted Manuscript

This article can be cited before page numbers have been issued, to do this please use: K. Mao, X. Cong, L. Feng, H. Chen, J. Wang, C. Wu, K. Liu, C. Xiao, Y. Yang and T. Sun, *Biomater. Sci.*, 2019, DOI: 10.1039/C9BM00226J.

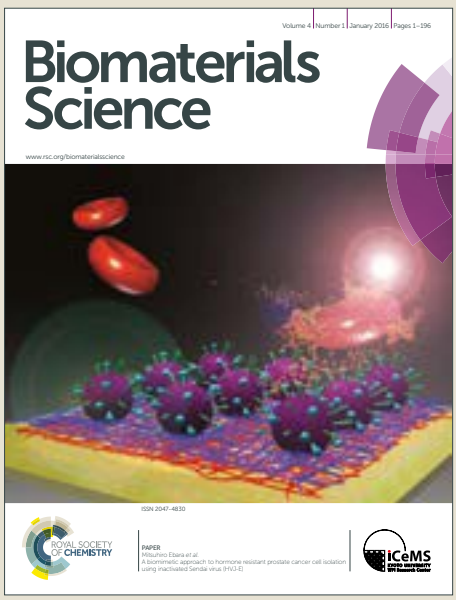

ROYAL SOCIETY OF CHEMISTRY

rsc.li/biomaterials-science

View Article Online
DOI: 10.1039/C9BM00226J

ARTICLE

Intratumoral Delivery of M-CSF by Calcium Crosslinked Polymer Micelles Enhances Cancer Immunotherapy

Received 00th January 20xx,
Accepted 00th January 20xx

DOI: 10.1039/x0xx00000x

Kuirong Mao[a,b,c,d,e,g], Xiuxiu Cong[a,b,c,d,e,g], Liangzhu Feng[i], Hongmei Chen[a], Jialiang Wang[a,b,c,d,e,g], Chenxi Wu[a], Kun Liu[i], Chunsheng Xiao[h], Yong-Guang Yang[a,b,c,d,e,f]* and Tianmeng Sun[a,b,c,d,e,g]*

Immunotherapy has shown promising results multiple malignancies. However, there are still significant challenges in cancer immunotherapy including the powerful immunosuppressive tumor microenvironment and adverse off-target side effects. Nanomaterials with defined physico-biochemical properties are versatile drug delivery platforms that may address these key technical challenges facing cancer immunotherapy. Here, a tumor acidity-responsive biomacromolecule delivery system was designed to intratumorally deliver an immune-activating cytokine, macrophage colony-stimulating factor (M-CSF) and attenuate the acidic microenvironment. This nanoparticle was prepared by introducing $CaCO_3$ as a crosslinker to form an M-CSF-loaded stable micelle (NP/M-CSF/$CaCO_3$). Administration of NP/M-CSF/$CaCO_3$ significantly inhibited tumor growth by enhancing T cell-mediated anti-tumor immune responses and reversing the TAM-mediated immunosuppression. This study provides new avenues for cascade amplification of the antitumor effects by targeting the tumor microenvironment. This approach may also help avoid unwanted complications.

Introduction

Antitumor immunotherapy can treat cancer by generating or augmenting a durable and robust immune response[1]. It has broad potential and has been used to treat many different types of malignancies[2]. Unfortunately, tumor cells can evade immune surveillance through a variety of mechanisms and immunotherapies—particularly those directed against solid tumors. It has thus far only benefited a minority of patients[3, 4].

Studies have shown that effective immunotherapy is limited in many patients by the immunosuppressive tumor microenvironment (TME)[5, 6]. Suppression of the tumor-specific T cells is orchestrated by the activity of stromal myeloid and lymphoid cells in the tumor tissue. In particular, tumor-associated macrophages (TAMs)— defined as the M2 type—play a key role in promoting tumor growth while inhibiting the anti-tumor immune response[7-9].

The signaling axis mediated by macrophage colony-stimulating factor (M-CSF) and its cognate receptor (M-CSFR) is a key regulator of monocyte differentiation and generation as well as the activity of tissue-resident macrophages[10]. M-CSF is the main growth factor for monocyte production in bone marrow and is a potent chemotactic molecule for monocytes. It can prime or directly stimulate a range of monocyte/macrophage functions[11]. Tumors with a high percentage of M-CSF-expressing cells had marked monocyte infiltration[12].

Acidic extracellular pH is a major feature of tumors; extracellular acidification is mostly due to lactate secretion from anaerobic glycolysis[13-15]. Accumulating evidence shows that an acidic microenvironment is a regulator of immune cell phenotypes[16, 17]. The extracellular pH of tumor tissues was reported earlier to polarize macrophages into an M2-like phenotype[18-20]. Therefore, the tumor immunosuppressive microenvironment can be effectively reprogramed by reducing the acidic environment in tumors.

Nanotechnology-based delivery systems can carry drugs with different properties via physical entrapment. This leads to improved pharmacokinetics and biodistribution via enhanced permeability and retention (EPR) effects[21, 22]. This leads to

[a] The First Hospital of Jilin University, Changchun, Jilin, China;
[b] Institute of Immunology, Jilin University, Changchun, Jilin, China;
[c] International Center of Future Science, Jilin University, Changchun, Jilin, China;
[d] National-local Joint Engineering Laboratory of Animal Models for Human Diseases, Changchun, Jilin, China;
[e] Key Laboratory of Organ transplantation and reconstruction, Jilin University, Changchun, Jilin, China;
[f] Columbia Center for Translational Immunology, Columbia University College of Physicians and Surgeons, New York, NY, USA;
[g] State Key Laboratory of Supramolecular Structure and Materials, Jilin University, Changchun, Jilin, China;
[h] Key Laboratory of Polymer Ecomaterials, Changchun Institute of Applied Chemistry Chinese Academy of Sciences, Changchun, Jilin, China.
[i] Jiangsu Key Laboratory for Carbon-Based Functional Materials & Devices, Institute of Functional Nano & Soft Materials (FUNSOM), Soochow University, Suzhou, Jiangsu, China.
[j] State Key Laboratory of Supramolecular Structure and Materials, College of Chemistry, Jilin University, Changchun, China.
* Email: tsun41@jlu.edu.cn (T. Sun); yongg@jlu.edu.cn (Y.G. Yang).
† Footnotes relating to the title and/or authors should appear here.
Electronic Supplementary Information (ESI) available: [details of any supplementary information available should be included here]. See DOI: 10.1039/x0xx00000x

potentially enhanced anticancer effects[23-25]. However, we emphasize that hydrophilic cytokines must be released extracellularly after being delivered to the tumor tissue. Thus, the ideal nanotechnology-based drug delivery system should offer enhanced accumulation in the tumor and rapid/sufficient extracellular chemokine following systemic administration.

Calcium compounds such as calcium phosphate ($Ca_3(PO_4)_2$) and calcium carbonate ($CaCO_3$) have received increasing attention for nanomedicine applications because of their excellent biocompatibility and biodegradability[26, 27]. Furthermore, calcium crosslinking or mineralization of polymer micelles could enhance the stability of nanoparticles[28] and make the nanoparticles sensitive to the acidic tumor microenvironment[29-31].

Amphiphilic polypeptide-based block copolymers have attracted considerable attention because of their biocompatibility and biodegradability. This makes them highly desirable for anticancer drug delivery[32, 33]. Poly (ethylene glycol)-b-poly (glutamic acid) (PEG-b-PGA) block copolymers in particular can form a tumor acidity-responsive micelle via calcium[34]. Here, we report a tumor acidity-responsive biomacromolecule delivery system that uses $CaCO_3$ as a crosslinker. This tool delivers M-CSF into the tumor tissue and weakens the acidic microenvironment. These nano-drug carriers significantly inhibited tumor growth by inducing T-cell-mediated anti-tumor immune response and reversing the TAM-mediated immunosuppression. This study provides new avenues for cascade amplification of antitumor effects that in turn regulate the tumor microenvironment.

Experimental

Chemicals, antibodies and cells.

Dulbecco's modified eagle medium (DMEM), penicillin/streptomycin, L-glutamine, fetal bovine serum (FBS), collagenase Type IV and 0.25% trypsin were all purchased from Life technologies (Carlsbad, CA, USA). Aqua dead cell stain kit was obtained from Invitrogen (Carlsbad, CA, USA). Red blood cell lysis buffer was purchased from Solarbio (Beijing, China). $CaCl_2$, Na_2CO_3 and PVP40 were all purchased from Sigma Aldrich (Saint Louis, MS, USA). Fluorescence-labeled rat anti-mouse CD11b, CD11c, F4/80, Gr-1, I-A/I-E, CD80, CD206, CD45, CD3, CD4, CD25, Foxp3, CD8, CD19, NK1.1 monoclonal antibodies were obtained from Biolegend (San Diego, CA, USA) and BD Biosciences (Franklin Lakes, NJ, USA). TAT peptide was synthetized by China Peptides Co., Ltd. (Suzhou, China). Sulfo-Cy5 NHS ester was purchased from Xi'an Ruixi Biological Technology Co., Ltd. (Xi'an, China). The mouse melanoma cell line B16 was purchased from American Type Culture Collection (ATCC). B16 cells were cultured in DMEM supplemented with 10% FBS at 37 ^oC incubator with 5% CO_2.

Animals and tumor model.

Female C57BL/6 mice (6 - 8 weeks) were purchased from Charles River (Beijing, China) and raised in a specific pathogen-free environment with free access to food and water. All animals received care in compliance with the guidelines outlined in the Guide for the Care and Use of Laboratory Animals. All procedures were approved by the Jilin University Animal Care and Use Committee.

To establish B16 tumor model, C57BL/6 mice were subcutaneously injected with1 $\times$ 10^6 B16 cells into the right side of the back. After the tumor volume reached about 100 mm^3, the mice were used for subsequent experiments.

Preparation of the $CaCO_3$-crosslinked nanoparticles.

Poly (glutamic acid) (PGA_{20k}) was synthesized as described previously[35]. Briefly, 15 mg PGA were added into aqueous solution at pH = 8.0 and stirred at room temperature (RT) for 30 min. Then, 15 mg $CaCl_2$, 30 mg PVP40, and 5 μg M-CSF were added into the PGA solution and stirred for another 60 min. After that, 15 mg Na_2CO_3 were added into the mixture and stirred at RT overnight. Blank nanoparticles were prepared using the same preparation process without adding M-CSF. For preparing the Cy5-TAT loaded nanoparticles, 5 mg $CaCl_2$, 10 mg PVP40, and 200 μg Cy5-TAT were added into the PGA solution and stirred for 60 min. Then, 5 mg Na_2CO_3 were added into the mixture and stirred overnight. All nanoparticles were purified by centrifugation (15000 g, 10 min) and washed twice with sterile water. Size and zeta potential of NP/M-CSF/$CaCO_3$ and NP/$CaCO_3$ were monitored by a dynamic light scattering (DLS, ZetasizerNanoZS90, Malvern Instruments, Southborough, UK) at 25 ^oC. The loading efficiency of M-CSF by NP/M-CSF/$CaCO_3$ was analyzed using Cy5 labeled M-CSF and the Xenogen IVIS Lumina system.

***In vitro* drug release**

The nanoparticle NP/Cy5-TAT/$CaCO_3$ was suspended in PBS at pH 7.4 or pH 6.5 at 37 ^oC with gentle shaking. At predetermined time points, the NP/Cy5-TAT/$CaCO_3$ was centrifuged and resuspended with fresh PBS. The supernatant was collected and freeze-dried. The amount of Cy5-TAT in the supernatant solution was calculated from a standard curve quantified on an Xenogen IVIS Lumina system.

pH responsive of the NP/$CaCO_3$ nanoparticles.

The NP/$CaCO_3$ nanoparticles were incubated in PBS with different pH and measured the sizes by DLS. Then, NP/$CaCO_3$ nanoparticles were incubated in PBS with pH 6.5 for 5, 10, and 15 min. And the sizes of these nanoparticles were measured by DLS. The morphologies of NP/$CaCO_3$ nanoparticles after incubating in PBS at pH 7.4 or 6.5 were observed by a high-resolution transmission electron microscopy (HRTEM) operated at 200 kV (JEM-2100F, JEOL, Tokyo, Japan) and scanning electron microscopy (SEM) operated at 3 kV (SU8000, Hitachi, Tokyo, Japan).

Tumor accumulation and tissue distribution of Cy5-TAT loaded nanoparticles.

When the B16 tumor volumes were about 300 mm^3, NP/Cy5-TAT/$CaCO_3$, free Cy5-TAT, or PBS solution were intravenously injected into the tumor-bearing mice. The Cy5-TAT distribution in mice was detected at 1, 2, 4, and 6 hours after injection using a Xenogen IVIS Lumina system (Caliper Life Sciences, CA, USA). At 6 h post-injection, the mice were sacrificed and the solid tumors and other organs were collected and imaged by the Xenogen IVIS Lumina system. Results were analyzed using Living Image software (Caliper Life Sciences, CA, USA).

Tumor growth inhibition study.

The B16 tumor-bearing mice were randomized into 4 groups, and administrated with glucose, free M-CSF, NP/$CaCO_3$ or NP/M-CSF/$CaCO_3$ through tail vein for seven times, respectively. The dose of M-CSF for each injection was 50 μg/kg. Tumor volumes were measured every day and calculated according to the following formula: $V = (a \times b^2)/2$, where a and b represented the maximum length and the minimal width of tumors, respectively.

Histopathological analysis

The B16 tumor-bearing mice were administrated with glucose, free M-CSF, NP/$CaCO_3$ or NP/M-CSF/$CaCO_3$ by *i.v.* injection for seven times, respectively. The dose of M-CSF for each injection was 50 μg/kg. At the end of this experiment, main organs (heart, liver, lung, spleen, and kidney) were harvested and fixed in 4% paraformaldehyde for 24 h. Paraffin sections were prepared and stained with hematoxylin-eosin (H&E), and the tissue sections were observed and photographed with an optical microscope (IX71, Olympus, Tokyo, Japan).

Flow cytometer Analysis.

At the end of tumor growth inhibition experiment, the B16-bearing mice were sacrificed and tumors, blood, spleen and bone marrow were harvested. The tumors were cut into small pieces and digested into single cells using 0.01% collagenase IV solution. The dissolved tissue was centrifuged at 1650 rpm for 5 min. The pellet was re-suspended in FACS buffer (PBS containing 0.1% BSA) and sequentially filtered through 40 μm mesh filters to remove debris and cell segments. Cells from mouse spleens were isolated by grinding spleens through 40 μm filters. After red blood cell lysis, blood cells and splenic cells were washed and re-suspended in FACS buffer. Then the cells were stained with appropriate dilutions of various combinations of the following fluorescence-labeled antibodies: anti-CD11b, anti-CD11c, anti-F4/80, anti-Gr-1, anti-I-A/I-E, anti-CD86, anti-CD206, anti-CD45, anti-CD3, anti-CD4, anti-CD25, anti-Foxp3, anti-CD8, anti-CD19, and anti-NK1.1. The stained cells were acquired on a LSRII Flow Cytometer using BD FACSDiva software (BD Bioscience) and data were analyzed using Flowjo10 software.

Confocal laser scanning microscopy imaging.

Tumors were harvested from tumor-bearing mice at 6 h after administration with NP/Cy5-TAT/$CaCO_3$, free Cy5-TAT, or PBS. Tumors were fixed in 4% paraformaldehyde overnight and immersed overnight in 30% sucrose solution. These tumors were sliced into 5 μm thickness and stained with DAPI and AF488-phalloidin according the manuscript. Images were captured by a Zeiss LSM 880 confocal laser scanning microscope using a 40 objective (Carl Zeiss, Oberkochen, Germany).

Statistical analysis.

Data are represented as mean ± standard error. Differences were analyzed using one-way analysis of variance (ANOVA) and Student's t-test. Data with $p < 0.05$ was considered statistically significant.

Results and discussion

Preparation and characterization of $CaCO_3$-crosslinked, M-CSF-loaded PGA nanoparticles.

PGA is a water-soluble, anionic, biodegradable, and edible biopolymer. Unlike other synthetic polymers that have been tested in clinical studies, PGA is composed of naturally occurring L-glutamic acid linked via amide bonds rather than a nondegradable C-C backbone; the free γ-carboxyl group in each repeating unit of L-glutamic acid is negatively charged at neutral pH. Here, PGA was first utilized to interact with Ca^{2+} via electrostatic adsorption due to its carboxyl groups on the side chain. After loading with Ca^{2+} to form a PGA-Ca complex (PGA-Ca), CO_3^{2-} and M-CSF were subsequently introduced to complete the in situ crosslinking leading to PGA-M-CSF/$CaCO_3$ nanoparticles denoted here as NP/M-CSF/$CaCO_3$ (Figure 1A).

All syntheses were performed in an aqueous medium with no harmful solvents or catalysts[36]. Blank nanoparticles (NP/$CaCO_3$) were produced by the same preparation method without introducing M-CSF. Dynamic light scattering (DLS) analysis revealed that NP/M-CSF/$CaCO_3$ and NP/$CaCO_3$ exhibit different diameters (Figure 1B) and similar zeta potentials (Figure 1C). The hydrodynamic diameters were 512.4 ± 7.1 nm for NP/M-CSF/$CaCO_3$ and 507.6 ± 44.0 nm for NP/$CaCO_3$. The zeta potentials for NP/M-CSF/$CaCO_3$ and NP/$CaCO_3$ were -19.7 ± 0.3 mV and -20.4 ± 0.2 mV, respectively. The nanoparticle sizes significantly increased after loading M-CSF, because of the steric effects of M-CSF. It was found that the NP/M-CSF/$CaCO_3$ had a high drug loading efficiency of 41.9 ± 12.4% (Figure S1).

View Article Online DOI: 10.1039/C8BM00226J

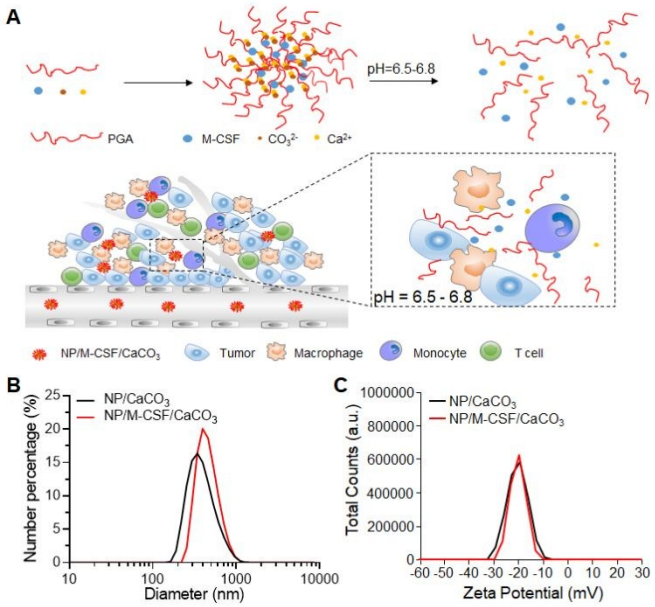

Figure 1. Characterization of $CaCO_3$ nanoparticles. (A) Schematic illustration of the preparation, selective accumulation in tumor tissue, and pH-triggered intratumoral drug release of the $CaCO_3$ crosslinked nanoparticle (NP/M-CSF/$CaCO_3$). (B) Particle sizes of NP/$CaCO_3$ and NP/M-CSF/$CaCO_3$. (C) The zeta potential of NP/$CaCO_3$ and NP/M-CSF/$CaCO_3$.

We further determined whether the $CaCO_3$-crosslinked nanoparticles responded to tumor extracellular pH *in vitro*. The NP/M-CSF/$CaCO_3$ was incubated in PBS at pH of 7.4, 6.5, or 4.5. Figure 2A showed that the milk-colored NP/M-CSF/$CaCO_3$ solution became lighter after incubation in a weakly acidic solution (pH = 6.5). It became transparent when added to a stronger acidic solution (pH = 4.5). Furthermore, the changes in diameters of NP/M-CSF/$CaCO_3$ after incubation in the pH 6.5 solution for 5, 10, and 15 min were measured by DLS. The diameter gradually decreased with increasing incubation time (Figure 2B).

HRTEM analysis revealed that NP/M-CSF/$CaCO_3$ changed from a spherical morphology with similar diameters to an irregular shape with significantly reduced diameter after incubation in a weakly acidic solution (pH = 6.5) (Figure 2C). To determine the structural changes of NP/M-CSF/$CaCO_3$ at pH 6.5, we observed the morphology by SEM. As shown in Figure 2D left, NP/M-CSF/$CaCO_3$ were uniform with about 500 nm and displayed a loose and rough surface at pH 7.4. While, the structure of NP/M-CSF/$CaCO_3$ was destroyed when the solution pH reduced to 6.5 (Figure 2D right). Then, the pH-boosted release of payload form drug loaded $CaCO_3$-crosslinked nanoparticle was further quantitatively evaluated (Figure 2E). A Cy5 labeled peptide (Cy5-TAT) was used as model biomacromolecule to prepare the nanoparticle (NP/Cy5-TAT/$CaCO_3$). It could be observed that only a small amount of Cy5-TAT was released from NP/Cy5-TAT/$CaCO_3$ after incubation in neutral solution (pH 7.4, approximately 25.2% at 8 h). In contrast, nearly 86.7% of the Cy5-TAT was released from NP/Cy5-TAT/$CaCO_3$ after incubating in acidic solution (pH 6.5) for 8 hours, indicating a boosted release of payload in the acidic environment of the tumor. These results demonstrated that the $CaCO_3$-crosslinked nanoparticle could be used as a tumor environment-responsive drug carrier for tumor-targeted drug delivery.

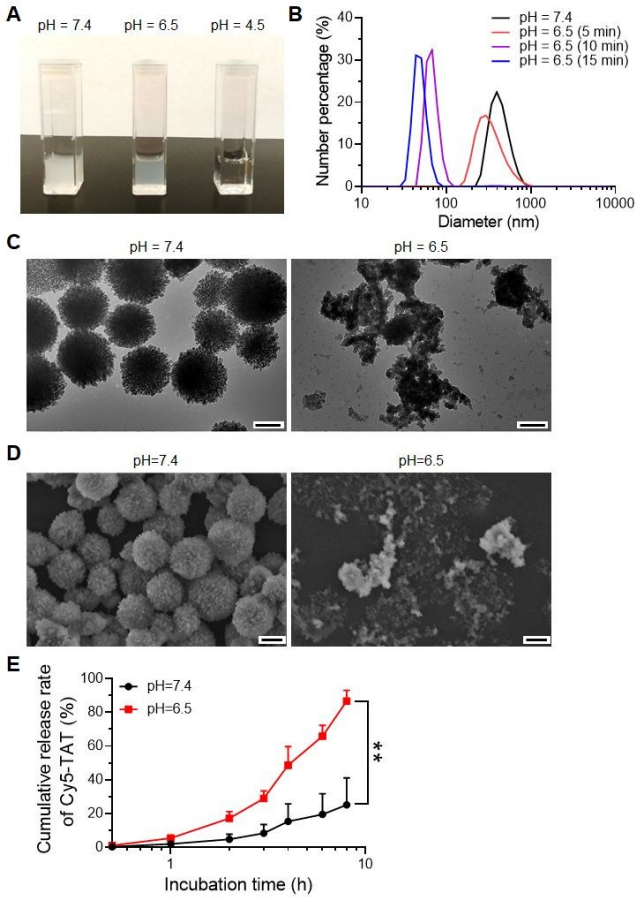

Figure 2. The pH response of NP/M-CSF/$CaCO_3$ *in vitro*. (A) Digital photographs demonstrating the pH-responsiveness of NP/M-CSF/$CaCO_3$ incubated in PBS of pH 7.4, 6.5 or 4.5. (B) Particle sizes of NP/M-CSF/$CaCO_3$ after incubating in PBS (pH 7.4 or 6.5) for different time (5, 10 or 15 min). (C) Representative HRTEM images of NP/M-CSF/$CaCO_3$ after incubating in PBS of pH 7.4 (left) or 6.5 (right). Scale bar = 500 nm. (D) Representative SEM images of NP/M-CSF/$CaCO_3$ after incubating in PBS of pH 7.4 (left) or 6.5 (right). Scale bar = 200 nm. (E) The cumulative release of Cy5-TAT from NP/Cy5-TAT/$CaCO_3$ incubated in neutral (pH 7.4) or acidic (pH 6.5) solution. Data are presented as mean ± SD (n = 3 per group).

The PGA/$CaCO_3$ nanoparticles accumulate in the tumor tissue and release their payload into the tumor stroma.

To determine the ability of the tumor pH-responsive nanoparticles to deliver hydrophilic biomacromolecules into the tumor stroma, we used the NP/Cy5-TAT/$CaCO_3$ and examined their biodistribution using a murine melanoma tumor model created by injecting B16 cells subcutaneously in

C57BL/6 mice. One hour after the injection, the NP/Cy5-TAT/$CaCO_3$ had already significantly accumulated in the tumor site with obvious and stable Cy5 fluorescent signal detected over the following 5 h, compared to that of PBS or free Cy5-TAT (Figure 3A). The Cy5 fluorescence of free Cy5-TAT or NP/Cy5-TAT/$CaCO_3$ also accumulated in the abdomen and bladder of mice as the circulation time increased (Figure 3A). In addition, heart, lung, liver, spleen, and kidney showed obvious accumulation of Cy5-TAT in mice treated with free Cy5-TAT or NP/Cy5-TAT/$CaCO_3$ after 6 h circulation (Figure 3B). Confocal laser scanning microscopy (CLSM) images of the tumor sections revealed accumulation of drug-loaded nanoparticles in the tumor (Figure 3C). No Cy5 fluorescence was detected in tumors from mice treated with PBS (Figure 3C). And few Cy5 fluorescence was observed in free Cy5-TAT treated tumor (Figure 3C). In contrast, tumors from mice treated with NP/Cy5-TAT/$CaCO_3$ had strong Cy5 fluorescence with most of the signal distributed in the intercellular space (yellow arrows in Figure 3C) and very few NP/Cy5-TAT/$CaCO_3$ distributed in the cytoplasm (white arrows in Figure 3C), demonstrating that the drug loaded tumor pH-responsive nanoparticles released their payloads rapidly and efficiently after penetrating into the tumor tissue from blood. However, almost all NP/Cy5-TAT/$CaCO_3$ nanoparticles distributed in the cytoplasm in the spleen (Figure 3D). And very few Cy5 fluorescence was detected in free Cy5-TAT treated spleen (Figure 3D). These results indicated that the $CaCO_3$-crosslinked nanoparticle could be used to effectively deliver biomacromolecules into the tumor extracellular matrix.

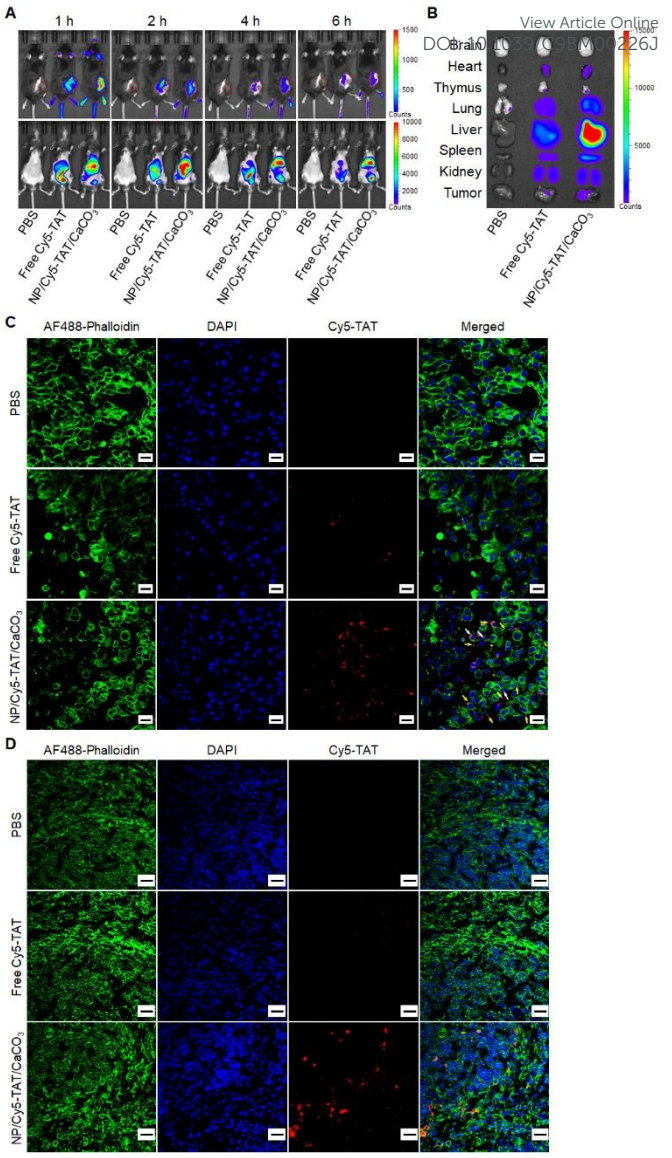

Figure 3. The biodistribution of NP/M-CSF/$CaCO_3$ *in vivo*. (A) Fluorescence images of B16-bearing mice after intravenous injection of PBS, free Cy5-TAT, or NP/Cy5-TAT/$CaCO_3$ at different time points. The tumor sites are denoted by red circles. (B) Fluorescence image of brains, hearts, thymus, lungs, livers, spleens, kidneys and tumors harvested at 6 h after *i.v.* injection of PBS, free Cy5-TAT, or NP/Cy5-TAT/$CaCO_3$. (C, D) CLSM images show the distribution of Cy5-TAT in tumor tissue (C) and spleen (D) at 6 h after *i.v.* injection of PBS, free Cy5-TAT, or NP/Cy5-TAT/$CaCO_3$. Cell nucleus were stained with DAPI (blue), cell membrane was stained with AF488-phalloidin (green). Yellow arrows, extracellular distribution of Cy5-TAT. White arrows, intracellular distribution of Cy5-TAT. Scale bar = 20 μm.

The NP/M-CSF/$CaCO_3$ nanoparticles significantly inhibit tumor growth by inducing anti-tumor immune responses.

To investigate the *in vivo* antitumor efficacy of M-CSF-encapsulated PGA/$CaCO_3$ nanoparticles, we administrated B16

tumor-bearing mice with glucose control, free M-CSF, NP/$CaCO_3$, or NP/M-CSF/$CaCO_3$ (once daily for 7 times). Figure 4A shows a significant inhibition of B16 tumor growth in mice that received NP/M-CSF/$CaCO_3$ injection versus those treated with NP/$CaCO_3$ (p = 0.0354), free M-CSF (p = 0.0193), or glucose control (p = 0.0347). The NP/$CaCO_3$ or free M-CSF did not significantly inhibit tumor growth compared to glucose control (p = 0.797 and 0.4537, respectively). Furthermore, mice in all groups survived to the end of the experiments with no significant changes in their body weight (Figure 4B), indicating that the $CaCO_3$-crosslinked nanoparticles with or without M-CSF encapsulation had no toxicity to mice.

To understand the mechanisms of the anti-tumor immune responses triggered by NP/M-CSF/$CaCO_3$ nanoparticles, we evaluated the changes in tumor immune microenvironment at the end of tumor growth inhibition experiment using flow cytometry. Compared to glucose control, mice treated with NP/M-CSF/$CaCO_3$ showed significant increases in the levels of $CD8^+$ T cells (Figure 4C) and ratio of $CD8^+/CD4^+$ in the tumor (Figure 4D), implicating an improved antitumor T cell response in these mice. Administration of NP/$CaCO_3$ or free M-CSF did not affect the ratio of $CD8^+/CD4^+$ in the tumor (Figure 4C).

The macrophage M1/M2 polarization balance in tumor influences the immunosuppressive tumor microenvironment[37]. Accumulating evidence shows that the extracellular pH of tumor tissues may polarize macrophages into an M2-like phenotype[18-20]. The ratio of M1/M2 polarization was significantly increased in NP/M-CSF/$CaCO_3$-treated tumors; however, it was completely unaffected by treatment with NP/$CaCO_3$ or free M-CSF (Figure 4E). These data indicate that intratumorally delivered $CaCO_3$ and M-CSF may act synergistically in polarizing macrophages into the M1 type, modulating the tumor microenvironment favoring the activation of anti-immune responses.

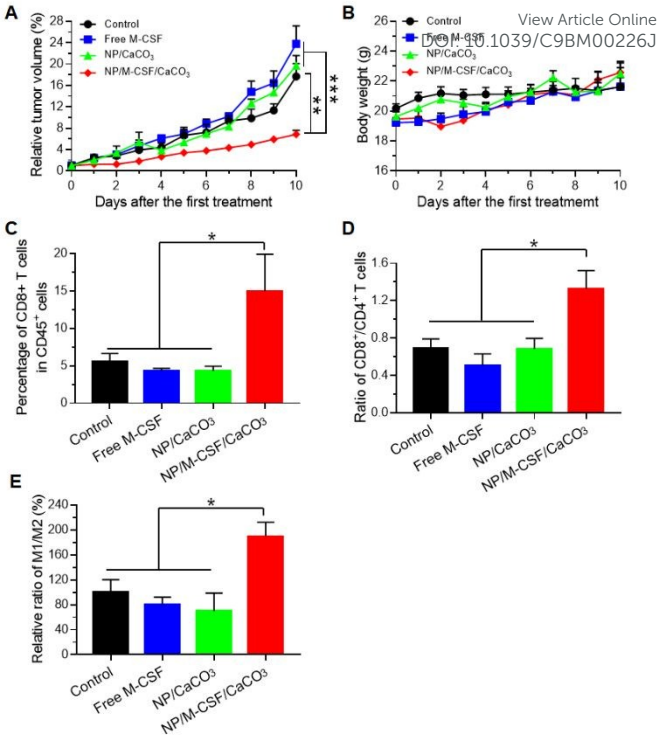

Figure 4. NP/M-CSF/$CaCO_3$ significantly inhibits B16 tumor growth and through enhanced anti-tumor immune responses. (A) Tumor growth was measured every day from the first treatment. Glucose control, free M-CSF, NP/$CaCO_3$ and NP/M-CSF/$CaCO_3$ were given by *i.v.* injection every day for 7 times from the tumor volume reached about 100 mm^3. The dose of M-CSF for each injection was 50 μg/kg (n = 5 per group). (B) The body weights of B16 tumor-bearing mice in the tumor inhibition experiment (n = 5 per group). (C to E) Frequencies of $CD8^+$ T cells (C) and the ratios of $CD8^+/CD4^+$ T cells (D) and M1 ($CD80/86^+$)/M2 ($CD206^+$) macrophages (E) in tumors were measured at the end of the tumor inhibition experiment (n = 5 per group). Data are presented as mean ± SD. *, $p < 0.05$; **, $p < 0.01$; ***, $p < 0.001$.

Finally, we demonstrated that whether the treatment of NP/M-CSF/$CaCO_3$ caused side effects. Various tissues, including heart, lungs, livers, spleens, and kidneys, were harvested from PBS-, free M-CSF-, NP/ $CaCO_3$-, or NP/M-CSF/$CaCO_3$-treated mice, and analyzed histologically for toxicity. The histological findings of the tissues collected from mice at the end of the therapeutic experiment are shown in Figure S2. All tissues from mice treated with free M-CSF, NP/ $CaCO_3$, or NP/M-CSF/$CaCO_3$ appeared normal, similar to those of the PBS controls that demonstrated no detectable toxicity. Then, we studied whether NP/M-CSF/$CaCO_3$ can induce changes in the systemic immune system by measuring the proportions of immune cell subsets in the blood and spleen using flow cytometry. Compared to glucose controls, administration of free M-CSF, NP/$CaCO_3$, or NP/M-CSF/$CaCO_3$ had negligible effects on the frequencies of CD4 T cells, CD8 T cells, and NK cells in the peripheral blood of B16 tumor-bearing mice. Free M-CSF caused a significant decrease in the frequency of B cells, which was not observed in the NP/$CaCO_3$-

View Article Online
DOI: 10.1039/C9BM00226J

or NP/M-CSF/$CaCO_3$-treated mice. In addition, there was an increase in the ratio of M1/M2 macrophage in peripheral blood of mice administrated with free M-CSF or NP/$CaCO_3$ (Figure 5B), but not in NP/M-CSF/$CaCO_3$-injected mice (Figure 5B). Furthermore, administration of free M-CSF, NP/$CaCO_3$, or NP/M-CSF/$CaCO_3$ did not significantly affect these immune cell subsets in the spleen (Figure 5C and D). These results demonstrate that delivery M-CSF using the tumor pH-responsive PGA/$CaCO_3$ nano-carrier enhances the antitumor responses with the tumor, while does not significantly affect the systemic immune responses.

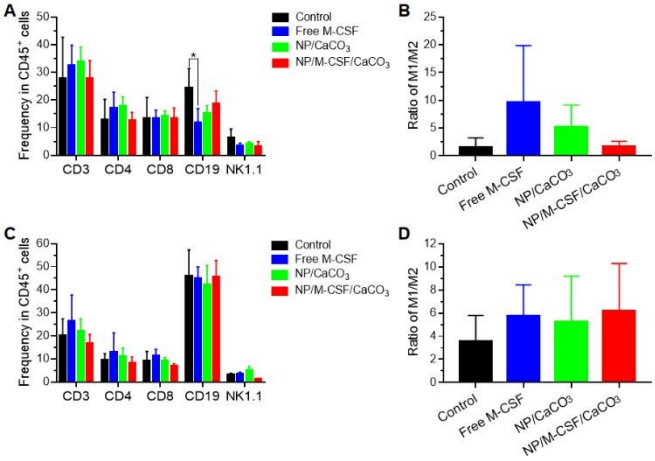

Figure 5. NP/M-CSF/$CaCO_3$ does not affect the immune cell frequencies in blood or spleen of B16 tumor-bearing mice. Glucose control, free M-CSF, NP/$CaCO_3$ and NP/M-CSF/$CaCO_3$ were given by *i.v.* injection every day for 7 times from the tumor volume reached about 100 mm^3. The dose of M-CSF for each injection was 50 μg/kg (n = 5 per group). The immune cells were measured at the end of the tumor inhibition experiment. (A) Frequencies of $CD3^+$ T cells, $CD4^+$ T cells, $CD8^+$ T cells, B cells and NK cells in $CD45^+$ cells in blood. (B) The ratios of M1 (IA/IE^+CD206^-)/M2 (IA/IE^-CD206^+) macrophages[38] in blood were measured at the end of the tumor inhibition experiment (n = 5 per group). (C) Frequencies of $CD3^+$ T cells, $CD4^+$ T cells, $CD8^+$ T cells, B cells and NK cells in $CD45^+$ cells in spleen. (D) The ratios of M1 (IA/IE^+CD206^-)/M2 (IA/IE^-CD206^+) macrophages[38] in spleen were measured at the end of the tumor inhibition experiment (n = 5 per group). Data are presented as mean ± SD. *, $p < 0.05$.

Conclusions

In summary, we established a "smart" nanoparticle delivery system that can release M-CSF proteins in the tumor tissue and attenuate the tumor acidic environment. The payloads quickly accumulated in the tumor after *i.v.* injection and were mainly released in tumor stroma, due to the nanoparticle's acid-sensitivity and stability in circulation. In addition, the calcium-crosslinked polymer micelles also inhibit the acidic environment of the tumor by reacting with the acidic components. Administration of the M-CSF-loaded calcium crosslinked nanoparticles significantly inhibited the tumor growth by prooting T-cell tumor infiltration and reversing the M1/M2 polarization balance in the tumor microenvironment. Our study provides new avenues for cascade amplifying the antitumor effects and regulating the tumor microenvironment.

Conflicts of interest

There are no conflicts to declare.

Acknowledgements

This work was supported by grants from Chinese MOST (2015CB964400), National Key Research and Development Program of China (2017YFA0208100), NSFC (81571798, 81422026, 91642208, 81871478), Program for Changjiang Scholars and Innovative Research Team in University (IRT_15R24), Special Fund Project of Jilin Province Provincial Industrial Innovation (2018C052-1).

References

[1] E. Ben-Akiva, S. Est Witte, R.A. Meyer, K.R. Rhodes, J.J. Green, Polymeric micro- and nanoparticles for immune modulation, Biomaterials science 7(1) (2018) 14-30.
[2] D.N. Khalil, E.L. Smith, R.J. Brentjens, J.D. Wolchok, The future of cancer treatment: immunomodulation, CARs and combination immunotherapy, Nature reviews. Clinical oncology 13(6) (2016) 394.
[3] M.S. Goldberg, Immunoengineering: how nanotechnology can enhance cancer immunotherapy, Cell 161(2) (2015) 201-4.
[4] D.S. Vinay, E.P. Ryan, G. Pawelec, W.H. Talib, J. Stagg, E. Elkord, T. Lichtor, W.K. Decker, R.L. Whelan, H. Kumara, E. Signori, K. Honoki, A.G. Georgakilas, A. Amin, W.G. Helferich, C.S. Boosani, G. Guha, M.R. Ciriolo, S. Chen, S.I. Mohammed, A.S. Azmi, W.N. Keith, A. Bilsland, D. Bhakta, D. Halicka, H. Fujii, K. Aquilano, S.S. Ashraf, S. Nowsheen, X. Yang, B.K. Choi, B.S. Kwon, Immune evasion in cancer: Mechanistic basis and therapeutic strategies, Semin Cancer Biol 35 Suppl (2015) S185-S198.
[5] D.H. Munn, V. Bronte, Immune suppressive mechanisms in the tumor microenvironment, Current opinion in immunology 39 (2016) 1-6.
[6] Z.B. Zhao, J. Long, Y.Y. Zhao, J.B. Yang, W. Jiang, Q.Z. Liu, K. Yan, L. Li, Y.C. Wang, Z.X. Lian, Adaptive immune cells are necessary for the enhanced therapeutic effect of sorafenib-loaded nanoparticles, Biomaterials science 6(4) (2018) 893-900.
[7] J.M. Brown, L. Recht, S. Strober, The Promise of Targeting Macrophages in Cancer Therapy, Clinical cancer research : an official journal of the American Association for Cancer Research 23(13) (2017) 3241-3250.
[8] P.J. Murray, Macrophage Polarization, Annu Rev Physiol 79 (2017) 541-566.
[9] B. Zheng, Y. Bai, H. Chen, H. Pan, W. Ji, X. Gong, X. Wu, H. Wang, J. Chang, Targeted delivery of tungsten oxide nanoparticles for multifunctional anti-tumor therapy via macrophages, Biomaterials science 6(6) (2018) 1379-1389.
[10] D.C. Strachan, B. Ruffell, Y. Oei, M.J. Bissell, L.M. Coussens, N. Pryer, D. Daniel, CSF1R inhibition delays cervical and mammary tumor growth in murine models by attenuating the turnover of

tumor-associated macrophages and enhancing infiltration by CD8(+) T cells, Oncoimmunology 2(12) (2013) e26968.
[11] K. Miyazaki, N.M. Isbel, H.Y. Lan, M. Hattori, K. Ito, M. Bacher, R. Bucala, R.C. Atkins, D.J. Nikolic-Paterson, Up-regulation of macrophage colony-stimulating factor (M-CSF) and migration inhibitory factor (MIF) expression and monocyte recruitment during lipid-induced glomerular injury in the exogenous hypercholesterolaemic (ExHC) rat, Clin Exp Immunol 108(2) (1997) 318-23.
[12] S.M. Scholl, C. Pallud, F. Beuvon, K. Hacene, E.R. Stanley, L. Rohrschneider, R. Tang, P. Pouillart, R. Lidereau, Anti-colony-stimulating factor-1 antibody staining in primary breast adenocarcinomas correlates with marked inflammatory cell infiltrates and prognosis, J Natl Cancer Inst 86(2) (1994) 120-6.
[13] Y. Kato, S. Ozawa, C. Miyamoto, Y. Maehata, A. Suzuki, T. Maeda, Y. Baba, Acidic extracellular microenvironment and cancer, Cancer Cell Int 13(1) (2013) 89.
[14] Q. Sun, C. Tang, Z. Su, J. Du, Y. Shang, L. Xue, C. Zhang, A modular assembly pH-sensitive charge reversal siRNA delivery system, Biomaterials science 6(11) (2018) 3075-3084.
[15] Y. Huang, J. Qin, J. Wang, G. Yan, X. Wang, R. Tang, Dual-stimuli-sensitive poly(ortho ester disulfide urethanes)-based nanospheres with rapid intracellular drug release for enhanced chemotherapy, Science China Chemistry 61(11) (2018) 13.
[16] V. Huber, C. Camisaschi, A. Berzi, S. Ferro, L. Lugini, T. Triulzi, A. Tuccitto, E. Tagliabue, C. Castelli, L. Rivoltini, Cancer acidity: An ultimate frontier of tumor immune escape and a novel target of immunomodulation, Semin Cancer Biol 43 (2017) 74-89.
[17] A.B. Hjelmeland, Q. Wu, J.M. Heddleston, G.S. Choudhary, J. MacSwords, J.D. Lathia, R. McLendon, D. Lindner, A. Sloan, J.N. Rich, Acidic stress promotes a glioma stem cell phenotype, Cell Death Differ 18(5) (2011) 829-40.
[18] A.E. El-Kenawi, A.A. Ibrahim-Hashim, K.A. Luddy, S.A. Pilon-Thomas, R.A. Gatenby, R.J. Gillies, Abstract 3213: Extracellular acidosis alters polarization of macrophages, Cancer research 75(15 Supplement) (2015) 3213-3213.
[19] A. El-Kenawi, C. Gatenbee, M. Robertson-Tessi, R. Bravo, J. Dhillon, Y. Balagurunathan, A. Berglund, N. Visvakarma, A. Ibrahim-Hashim, J. Choi, K. Luddy, R. Gatenby, S.P. Thomas, A. Anderson, B. Ruffell, R. Gillies, Acidity promotes tumor progression by altering macrophage phenotype in prostate cancer, (2018).
[20] O.R. Colegio, N.Q. Chu, A.L. Szabo, T. Chu, A.M. Rhebergen, V. Jairam, N. Cyrus, C.E. Brokowski, S.C. Eisenbarth, G.M. Phillips, G.W. Cline, A.J. Phillips, R. Medzhitov, Functional polarization of tumour-associated macrophages by tumour-derived lactic acid, Nature 513(7519) (2014) 559-63.
[21] L. He, W. Xu, X. Wang, C. Wang, J. Ding, X. Chen, Polymer micro/nanocarrier-assisted synergistic chemohormonal therapy for prostate cancer, Biomaterials science 6(6) (2018) 1433-1444.
[22] H. Chen, Z. Gu, H. An, C. Chen, J. Chen, C. R, S. Chen, W. Chen, X. Chen, X. Chen, Z. Chen, B. Ding, Q. Dong, Q. Fan, T. Fu, D. Hou, Q. Jiang, H. Ke, X. Jiang, G. Liu, S. Li, T. Li, Z. Liu, G. Nie, M. Ovais., D. Pang, N. Qiu, Y. Shen, H. Tian, C. Wang, H. Wang, Z. Wang, H. Xu, J. Xu, X. Yang, S. Zhu, X. Zheng, X. Zhang, Y. Zhao, W. Tan, X. Zhang, Y. Zhao, Precise nanomedicine for intelligent therapy of cancer, Science China Chemistry 61(12) (2018) 50.
[23] X.Z. Yang, X.J. Du, Y. Liu, Y.H. Zhu, Y.Z. Liu, Y.P. Li, J. Wang, Rational design of polyion complex nanoparticles to overcome cisplatin resistance in cancer therapy, Adv Mater 26(6) (2014) 931-6.
[24] M.E. Davis, Z.G. Chen, D.M. Shin, Nanoparticle therapeutics: an emerging treatment modality for cancer, Nature reviews. Drug discovery 7(9) (2008) 771-82.
[25] R.K. Jain, T. Stylianopoulos, Delivering nanomedicine to solid tumors, Nature reviews. Clinical oncology 7(11) (2010) 653-64.
[26] S. Maleki Dizaj, M. Barzegar-Jalali, M.H. Zarrintan, K. Adibkia, F. Lotfipour, Calcium carbonate nanoparticles as cancer drug delivery system, Expert Opin Drug Deliv 12(10) (2015) 1649-60.
[27] D.B. Trushina, T.V. Bukreeva, M.V. Kovalchuk, M.N. Antipina, CaCO(3) vaterite microparticles for biomedical and personal care applications, Mater Sci Eng C Mater Biol Appl 45 (2014) 644-58.
[28] K.K. Perkin, J.L. Turner, K.L. Wooley, S. Mann, Fabrication of hybrid nanocapsules by calcium phosphate mineralization of shell cross-linked polymer micelles and nanocages, Nano Lett 5(7) (2005) 1457-61.
[29] K.H. Min, H.S. Min, H.J. Lee, D.J. Park, J.Y. Yhee, K. Kim, I.C. Kwon, S.Y. Jeong, O.F. Silvestre, X. Chen, Y.S. Hwang, E.C. Kim, S.C. Lee, pH-controlled gas-generating mineralized nanoparticles: a theranostic agent for ultrasound imaging and therapy of cancers, ACS Nano 9(1) (2015) 134-45.
[30] Z. Dong, L. Feng, W. Zhu, X. Sun, M. Gao, H. Zhao, Y. Chao, Z. Liu, CaCO3 nanoparticles as an ultra-sensitive tumor-pH-responsive nanoplatform enabling real-time drug release monitoring and cancer combination therapy, Biomaterials 110 (2016) 60-70.
[31] M.F. Chung, W.T. Chia, W.L. Wan, Y.J. Lin, H.W. Sung, Controlled Release of an Anti-inflammatory Drug Using an Ultrasensitive ROS-Responsive Gas-Generating Carrier for Localized Inflammation Inhibition, Journal of the American Chemical Society 137(39) (2015) 12462-5.
[32] L. Zhao, N. Li, K. Wang, C. Shi, L. Zhang, Y. Luan, A review of polypeptide-based polymersomes, Biomaterials 35(4) (2014) 1284-301.
[33] Z. Guo, X. Zhou, M. Xu, H. Tian, X. Chen, M. Chen, Dimeric camptothecin-loaded RGD-modified targeted cationic polypeptide-based micelles with high drug loading capacity and redox-responsive drug release capability, Biomaterials science 5(12) (2017) 2501-2510.
[34] P. Mi, D. Kokuryo, H. Cabral, H. Wu, Y. Terada, T. Saga, I. Aoki, N. Nishiyama, K. Kataoka, A pH-activatable nanoparticle with signal-amplification capabilities for non-invasive imaging of tumour malignancy, Nature nanotechnology 11(8) (2016) 724-30.
[35] C.X. J. Ding, L. Zhao, Y. Cheng, L. Ma, Z. Tang, X. Zhuang, X. Chen, Poly(L - glutamic acid) grafted with oligo(2 - (2 - (2 - methoxyethoxy)ethoxy)ethyl methacrylate): Thermal phase transition, secondary structure, and self - assembly, Journal of Polymer Science Part A: Polymer Chemistry 49(12) (2011) 13.
[36] L.C. Yi Zhang, Di Li, Yeh-Hsing Lao, Dingzhuo Liu, Mingqiang Li, Jianxun Ding, Xuesi Chen, Tumor microenvironment-responsive hyaluronate-calciumcarbonate hybrid nanoparticle enables effective chemo-therapy for primary and advanced osteosarcomas, Nano Research 11(9) (2018) 17.
[37] Z. Li, M. Zhao, T. Li, J. Zheng, X. Liu, Y. Jiang, H. Zhang, X. Hu, Decidual Macrophage Functional Polarization during Abnormal Pregnancy due to Toxoplasma gondii: Role for LILRB4, Frontiers in immunology 8 (2017) 1013.
[38] D. Daley, V.R. Mani, N. Mohan, N. Akkad, G. Pandian, S. Savadkar, K.B. Lee, A. Torres-Hernandez, B. Aykut, B. Diskin, W. Wang, M.S. Farooq, A.I. Mahmud, G. Werba, E.J. Morales, S. Lall, B.J. Wadowski, A.G. Rubin, M.E. Berman, R. Narayanan, M. Hundeyin, G. Miller, NLRP3 signaling drives macrophage-induced adaptive immune suppression in pancreatic carcinoma, The Journal of experimental medicine 214(6) (2017) 1711-1724.

View Article Online
DOI: 10.1039/C9BM00226J

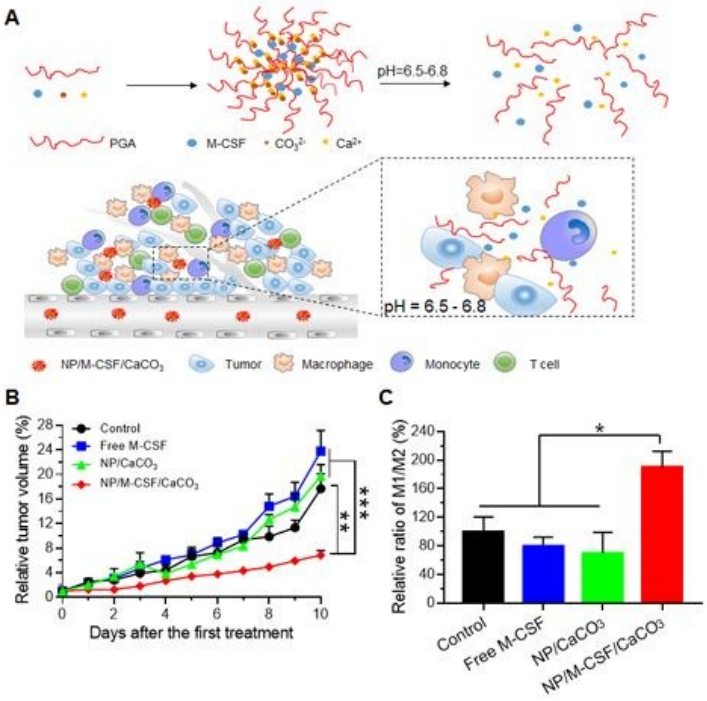

This study provides new avenues for cascade amplification of the antitumor effects by regulating the tumor microenvironment.